World Scientific
www.worldscientific.com

ON THE GAMMA-RAY EMISSION FROM THE CORE AND RADIO LOBES OF THE RADIO GALAXY CENTAURUS A*

NAREK SAHAKYAN[†,¶], FRANK M. RIEGER[‡] and FELIX AHARONIAN[‡,§]

[†]*ICRANet-Yerevan, Marshall Baghramian Avenue, 24, Yerevan 0019, Republic of Armenia*
and
ICRANet, Piazza della Repubblica 10, I-65122 Pescara, Italy

[‡]*Max-Planck-Institut für Kernphysik, P.O. Box 103980, 69029 Heidelberg, Germany*

[§]*Dublin Institute for Advanced Studies, 31 Fitzwilliam Place, Dublin 2, Ireland*
[¶]*narek@icra.it*

RUIZHI YANG[‖] and EMMA DE ONA-WILHELMI[**]

[‖]*Key Laboratory of Dark Matter and Space Astronomy, CAS, Nanjing, 210008, China*

[**]*Institut de Cincies de l'Espai (IEEC-CSIC), Barcelona 08193, Spain*

We summarize recent results based on an analysis of Fermi-LAT data for the lobes and the core of the nearby radio galaxy Centaurus A (Cen A). In the case of the *core*, high-energy (HE; > 100 MeV) γ-rays up to 50 GeV have been detected with a detection significance of about 44σ. The average gamma-ray spectrum of the core reveals interesting evidence for a possible deviation from a simple power-law. A likelihood analysis with a broken power-law model shows that the photon index becomes substantially harder above $E_b \simeq 4$ GeV, changing from $\Gamma_1 = 2.74 \pm 0.03$ below to $\Gamma_2 = 2.09 \pm 0.20$ above. It seems possible that this hardening marks the contribution of an additional high-energy component beyond the common synchrotron-self Compton jet emission.

In the case of the *lobes*, the high-energy gamma-ray emission extends up to 6 GeV, with a significance of more than 10 and 20 σ for the north and the south lobe, respectively. Based on a detailed spatial analysis and comparison with the associated radio lobes, a substantial extension of the HE γ-ray emission beyond the WMAP radio image for the northern lobe of Cen A is found. We provide a short discussion of the lobe's spectral energy distribution (SED) in the context of hadronic and time-dependent leptonic scenarios.

Keywords: Galaxies: active; galaxies: Cen A, gamma rays, radiation mechanisms: non-thermal.

PACS Numbers: 98.54.Gr, 95.85.Pw, 95.30.Gv

1. Introduction

The prominent radio galaxy Centaurus A (NGC 5128), at a distance of $\simeq$ 3.8 Mpc,[1] is our closest active galaxy. Often considered as a prototype Fanaroff-Riley Class I[2] radio source and as a misaligned BL Lac-type object at higher energies,[3,4] it is one of the best-studied extragalactic objects over a wide range of frequencies.[5] Observations at radio frequencies show giant structures (so-called 'lobes') with a total angular size of $\sim 10°$, which corresponds to a physical extension of ~ 600 kpc (d/3.8 Mpc).

The Fermi-LAT collaboration has early on reported the detection of HE γ-rays from both the core (i.e., within $\sim 0.1°$) and the giant radio lobes of Cen A:[6,7] An analysis of the available ten-month LAT data set revealed a point-like HE emission region coincident with the position of the radio core of Cen A, and two large extended emission regions detected with a significance of 5 and 8σ for the northern and the southern lobe, respectively. On the other hand, the HE emission from the extended regions seemed to be morphologically correlated with the giant radio lobes, contributing more than 50 % to the total HE source emission. These regions appeared spectrally well described by a power-law function extending up to 2 or 3 GeV with photon indices of $\Gamma \sim 2.6$.

Here we report on our results obtained using a much larger Fermi-LAT data set, allowing for a detailed investigation of the spectrum and morphology of the 'lobes' and for an improved analysis of the spectral and temporal characteristics of HE core emission.

2. Fermi-LAT Data Analysis

Here we present the main observational results of a Fermi-LAT analysis of HE core and lobe emission in Cen A. Detailed information on the analysis can be found in Refs. 8, 9.

2.1. *The core of Cen A*

The continuum gamma-ray emission of the core of Cen A has first been modeled with a single power law and a binned *gtlike* analysis been performed. The best-fit power-law parameters for the core of Cen A turned out to be

$$\left(\frac{dN}{dE}\right)_P = (2.73 \pm 0.12) \times 10^{-9} \left(\frac{E}{100 \text{ MeV}}\right)^{-2.69 \pm 0.03} . \tag{1}$$

The test statistic is $TS = 1978$ above 100 MeV, corresponding to a $\approx 44\sigma$ detection significance. Figure 1(a) shows the spectrum of the core of Cen A obtained by separately running *gtlike* for 12 energy bands, where the dashed line shows the best-fit single power-law function for the data given in Eq. (1). For the highest energy bin (56.2-100 GeV), an upper limit is shown. A closer inspection shows, however,
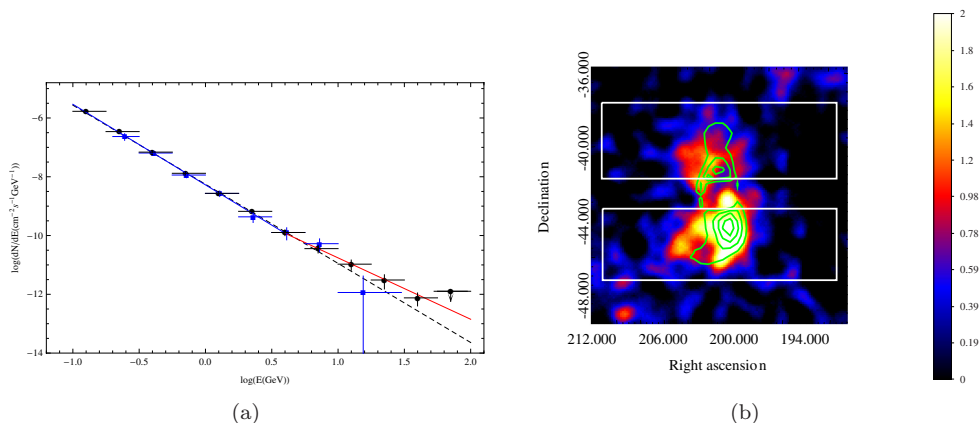
Fig. 1.   (a) Average high-energy gamma-ray (>100 MeV) spectrum of the core of Cen A. The power-law function from the Eq. (1) is depicted with dashed black line. (b) Cen A 'lobes': Excess map after subtraction of diffuse background, point-like sources and Cen A core.

that the measured spectrum exhibits clear deviations from a single power-law model with respect to the data above several GeV (χ^2 fit of the power-law model to the data gives a relatively poor fit with $\chi^2 = 39.7$ for 9 dof). In order to analyze this in more detail, the core spectrum has been modeled with a broken power-law model and *gtlike* tool retried. The best-fit broken power-law parameters are now

$$\left(\frac{dN}{dE}\right)_{BP} = (1.19 \pm 0.08) \times 10^{-13} \left(\frac{E}{E_b}\right)^{-\Gamma_{1,2}}, \tag{2}$$

with $\Gamma_1 = 2.74 \pm 0.02$ and $\Gamma_2 = 2.12 \pm 0.14$ below and above $E_b = (4.00 \pm 0.09)$ GeV, respectively. The power-law and the broken-power-law models can be compared using a log likelihood ratio test. The test statistic is twice the difference in these log-likelihoods, which gives 9 for this case. Note that the probability distribution of the test statistic can be approximated by a χ^2 distribution with 2 dof, corresponding to different degrees of freedom between the two functions. In this case $P(\chi^2) = 0.011$, which again indicates a deviation from a simple power-law function.

The results presented above indicate an interesting hardening of the (average) gamma-ray core spectrum towards higher energies. The break in the spectrum at 4 GeV could most naturally be explained by a superposition of different spectral components. If one divides the data set into two energy ranges, i.e., [0.1- 4] GeV and [4-100] GeV, modelling each energy range separately with a power-law function, the analysis gives a photon index of $\Gamma_1 = 2.74 \pm 0.02$ and a flux $F_\gamma = (1.68 \pm 0.04) \times 10^{-7}$ photon cm^{-2}s^{-1} for the [0.1-4] GeV interval (test statistics gives TS=1944) and $\Gamma_2 = 2.09 \pm 0.2$, and $F_\gamma = (4.20 \pm 0.64) \times 10^{-10}$ photon cm^{-2}s^{-1} for the [4-100] GeV range (TS value 124.4), respectively. These components are depicted with a blue and red line in Fig. 1(a).

2.2. *The lobes of Cen A*

For the analysis of Fermi-LAT data of the lobes events with energies between 200
MeV and 30 GeV were selected. Figure 1(b) shows the residual image obtained
after subtracting point like sources (including the core of Cen A) and the diffuse
background. In order to evaluate the total (extended) HE γ-ray emission in more
detail, a template based on the residual map (T1) has been used. The TS values
for the south and the north lobe in this template are 411 and 155, respectively.
Green contours in Fig. 1(b) show the radio lobes (WMAP, 22 GHz), with the higher-
frequency 22 GHz map being used as it better represents the GeV-emitting particles.
A closer inspections reveals that the south lobe of the HE γ-ray image is roughly
similar to the south lobe of the radio one, whereas the HE emission in the north
seems to extend beyond the radio lobe emission region Fig. 1(b). A morphological
analysis in fact indicates some incongruity between the morphology of the radio
lobe and γ-ray lobe in the north. This is particularly instructive as HE gamma-
rays directly trace the underlying spatial distribution of energetic electrons (via
IC processes) without the degeneracy involved in the radio synchrotron part (i.e.,
uncertainties in magnetic field topology). Using the template generated with the
residual map (T1), the total flux and photon index of the north and the south
lobe is derived for the energy range from 100 MeV to 30 GeV. For the north lobe,
the integral HE flux is $(0.93 \pm 0.09) \times 10^{-7}$ph cm^{-2}s^{-1} and the photon index is
2.24 ± 0.08, while for the south lobe we find $(1.4 \pm 0.2) \times 10^{-7}$ph cm^{-2}s^{-1} and
2.57 ± 0.07, respectively.

3. Discussion

The core of Cen A: The analysis of the 4 yr-data set interestingly reveals that the
HE core spectrum of Cen A shows an *unusual* break, with photon index changing
from $\simeq 2.7$ to $\simeq 2.1$ at an energy of $E_b \simeq 4$ GeV. While spectral breaks are often
associated with a situation where the spectrum gets softer, here the opposite occurs.
For the component below 4 GeV, the detected photon flux $F_\gamma = (1.68 \pm 0.04) \times$
10^{-7} photon cm^{-2}s^{-1} corresponds to an apparent (isotropic) γ-ray luminosity of
$L_\gamma(0.1 - 4 \text{ GeV}) \simeq 10^{41}$ erg s^{-1} (for the distance 3.8 Mpc). On the other hand,
the HE luminosity of the component above 4 GeV translates into $L_\gamma(> 4\text{GeV}) \simeq$
1.4×10^{40} erg s^{-1}. This is an order of magnitude less when compared with the
first component, but still larger than the VHE luminosity reported by H.E.S.S.
$L_\gamma(> 250 \text{ GeV}) = 2.6 \times 10^{39}$ erg s^{-1}.[10] In fact, the spectral hardening seen at GeV
energies may allow to account for the (non-simultaneous) H.E.S.S. flux data.

The limited angular resolution (~ 5 kpc) and the lack of significant variability
introduces substantial uncertainties as to the production site of the HE gamma-
ray emission. In principle, the hard HE component could originate from both a
very compact (sub-pc) and/or extended (multi-kpc) region(s). The double-peaked
nuclear SED of Cen A has in the past been reasonably well-modeled with simple
one zone SSC models up to a few GeV.[4,7] In this framework, the observed break at

4 GeV would indeed mark the appearance of a physically different component. This additional component could in principle be related to a number of different (not mutually exclusive) scenarios, from magnetosphere VHE emission[11] up to inverse Compton processes in the kpc-scale jet,[12] see Ref. 9 for a full discussion. At the current stage, none of these models can be easily discarded. Definite progress concerning the true origin of the HE gamma-ray could be achieved, however, in case of a significant detection of gamma-ray time variability.

The lobes of Cen A: The HE γ-ray emission observed from the lobes could in principle be related to leptonic (inverse-Compton scattering) or hadronic (e.g., pp-interaction) processes. In the following, we briefly summarize possible constraints for the underlying radiation mechanism imposed by the observed SEDs (for detailed information see Ref. 8). In a *leptonic scenario*, both the HE γ-ray and the radio emission could be satisfactorily accounted for. Assuming an electron injection spectrum with an exponential cut-off, the emergent electron distribution, found by solving the kinetic equation describing the energetic and temporal evolution of the radiating electrons, can been used to model the SED through synchrotron and inverse-Compton emission.

The duration of particle acceleration (associated with this the age of the giant lobe emission) is unknown. Dynamical arguments suggest a lower limit $> 10^7$ yr for the giant radio lobes, while synchrotron spectral ageing arguments indicate an age $\lesssim 3 \times 10^7$ yr.[5,13,14] In the following, we therefore discuss the SED implications for an epoch time t between 10^7 yr and 10^8 yr. As it turns out, the modeling of the GeV data provides support for a maximum lobe age of $\sim 8 \times 10^7$ yr.

Figure 2 shows a SED representation for an epoch time $t_{\max} = 8 \times 10^7$ yr (for the SED for $t = 10^7$ yr see Ref. 8), with a maximum electron Lorentz factor $\gamma_{\max} = 2.5 \times 10^6$ and 1.5×10^6 for the north lobe and the south lobe, respectively. Note that in this case the contribution by inverse-Compton scattering of CMB photons alone would be sufficient to account for the observed HE spectrum (see the
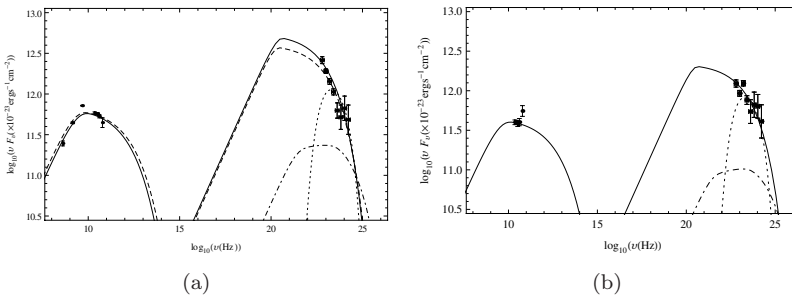

(a)   (b)

Fig. 2.   SED for $t = 8 \times 10^7$ yr and for a mean magnetic field value B for the south lobe and the γ-ray excess region in the north lobe of 0.91 μG and 1.17 μG, respectively. The dot-dashed line in (a) represents the IC contribution due to EBL upscattering while the dashed line shows the result for $t = 10^8$ yr. The possible γ-ray flux expected from pp-interactions given a thermal gas density $n = 10^{-4}$ cm^{-3} is also shown (dotted line).

solid line in Fig. 2). On the other hand, for an epoch time t exceeding $t_{\max} = 8 \times 10^7$ yr, the high-energy part of the SED would no longer be consistent with the data (see the dashed line in Fig. 2 for $t = 10^8$ yr). These considerations provide additional support for a finite age $< 10^8$ yr of the lobes. The maximum total energy of electrons in both lobes is found to be $\approx 6 \times 10^{57}$ erg, with the total energy in particles and fields comparable to the 10^7yr-case, thus requiring only a relatively modest mean kinetic jet power of $\sim 10^{43}$ erg/s.

In principle, a *hadronic origin* is conceivable as well: Once protons are efficiently injected, they are likely to remain energetic since the cooling time for pp-interactions is $t_{\mathrm{pp}} \approx 10^{15}(n/1 \ cm^{-3})^{-1}$ s. High-energy protons interacting with the ambient low-density plasma can then produce neutral pions which decays into two γ-rays. Similar to before, we employed a power-law proton distribution with an exponential cut-off to model the SED. Furthermore, a thermal plasma density $n = 10^{-4}$ cm^{-3} for the giant radio lobes of Cen A has been assumed. This model representation is depicted by a dotted line in Fig. 2. In both lobes, the power-law index of the proton population is $\alpha = 2.1$, and the high-energy cut-off is $E_{\max} \simeq 55$ GeV. The maximum total energy W_p is proportional to the gas number density n, so that $W_p \simeq 10^{61}(n/10^{-4} \ \mathrm{cm}^{-3})^{-1}$ erg, obtained here, should be considered as an upper limit.

4. Conclusions

We have highlighted recent results from HE observation of the radio galaxy Cen A. Accordingly, the core of Cen A shows a more complex spectral gamma-ray behavior than previously anticipated ("unusual" break at 4 GeV), while the HE γ-ray emission from the lobes do not fully coincide with the radio lobes (e.g., excess region in the north lobe). These results indicate that Cen A is a promising target for studies with the next generation HE/VHE γ-ray instruments (e.g. Cherenkov Telescope Array).

References

1. G. Harris, M. Rejkuba and W. Harris, *PASA* **27**, 457 (2010).
2. B. Fanaroff and J. Riley, *MNRAS* **167**, 31P (1974).
3. R. Morganti, R. Fosbury, R. Hook *et al.*, *MNRAS* **256**, 1P (1992).
4. M. Chiaberge, A. Capetti and A. Celotti, *MNRAS* **324**, L33 (2001).
5. F. Israel, *A&A Rev.* **8**, 237 (1998).
6. A. Abdo *et al.* (Fermi-LAT), *Science* **328**, 725 (2010a).
7. A. Abdo *et al.* (Fermi-LAT), *ApJ* **719**, 1433 (2010b).
8. R. Yang, N. Sahakyan, *et al.*, *A&A* **542**, A19 (2012).
9. N. Sahakyan, R. Yang, *et al.*, *ApJL* **770L**, 6S (2013).
10. F. Aharonian *et al.*, (H.E.S.S. Collaboration), *ApJ* **695**, L40 (2009).
11. F. Rieger, *IJMPD* **20**, 1547 (2011).
12. M. Hardcastle and J. Croston, *MNRAS* **415**, 133 (2011).
13. H. Alvarez, *et al.*, *A&A* **355**, 863 (2000).
14. M. Hardcastle, C. Cheung, I. Feain and L. Stawarz, *MNRAS* **393**, 104 (2009).